AFRL-AFOSR-VA-TR-2021-0009

The Molecular Mechanisms Responsible for the Assembly of Spider Silk Fibers

Holland, Gregory
SAN DIEGO STATE UNIVERSITY FOUNDATION
230 W 41ST STREET FL 7
NEW YORK, NY, 921821901
US

01/29/2021
Final Technical Report

Air Force Research Laboratory
Air Force Office of Scientific Research
Arlington, Virginia 22203
Air Force Materiel Command

REPORT DOCUMENTATION PAGE

Form Approved
OMB No. 0704-0188

1. REPORT DATE *(DD-MM-YYYY)*	**2. REPORT TYPE**	**3. DATES COVERED** *(From - To)*
29-01-2021	Final	01 Jun 2017 - 31 May 2020

4. TITLE AND SUBTITLE
The Molecular Mechanisms Responsible for the Assembly of Spider Silk Fibers

5a. CONTRACT NUMBER

5b. GRANT NUMBER
FA9550-17-1-0282

5c. PROGRAM ELEMENT NUMBER

6. AUTHOR(S)
Gregory Holland

5d. PROJECT NUMBER

5e. TASK NUMBER

5f. WORK UNIT NUMBER

7. PERFORMING ORGANIZATION NAME(S) AND ADDRESS(ES)
SAN DIEGO STATE UNIVERSITY FOUNDATION
230 W 41ST STREET FL 7
NEW YORK, NY 921821901
US

8. PERFORMING ORGANIZATION REPORT NUMBER

9. SPONSORING/MONITORING AGENCY NAME(S) AND ADDRESS(ES)
AF Office of Scientific Research
875 N. Randolph St. Room 3112
Arlington, VA 22203

10. SPONSOR/MONITOR'S ACRONYM(S)
AFRL/AFOSR RTB2

11. SPONSOR/MONITOR'S REPORT NUMBER(S)
AFRL-AFOSR-VA-TR-2021-0009

12. DISTRIBUTION/AVAILABILITY STATEMENT
A Distribution Unlimited: PB Public Release

13. SUPPLEMENTARY NOTES

14. ABSTRACT
The ability to replicate spider silk assembly in the laboratory continues to elude scientists. It is our belief that this is due to a lack of understanding regarding the molecular underpinnings for converting the protein-rich fluid in the spider's gland to an insoluble fiber with outstanding mechanical properties that exceed most man-made materials. This proposal describes a research plan designed to elucidate the molecular structure, dynamics and interactions of the silk proteins in the gland fluid and determine the important biochemical triggers responsible for converting this gel-like liquid to fibers with unparalleled, yet diverse mechanical properties. The need for such an understanding has been noted in the recent AFOSR funding opportunity, BAA-AFOSR-2015, Natural Materials, Systems and Extremophiles section, where an understanding of the mechanisms for natural directed assembly was highlighted (pp. 48-49). We propose to use a combination of nuclear magnetic resonance (NMR) approaches including solid-state NMR, high-resolution NMR and
Diffusion NMR techniques in conjunction with cryo-electron microscopy (cryo-EM) and X-ray diffraction to study the various spider silk producing glands in their native state and under different biochemical conditions. We aim to characterize the dynamics of the silk proteins within the glands where there is now strong evidence for oligomeric silk protein assembly. Some of this evidence comes from diffusion NMR and cryo-EM research we performed in our current (but ending) AFOSR grant. Recently, we succeeded in developing an approach to grow spider silk fibers directly from the gland fluid by changing the biochemical conditions such as pH. Much of the proposed work will involve characterizing the kinetics of silk fiber assembly with this approach and the molecular structure of the resulting fibers with a range of solid-state NMR and diffraction techniques. The proposed research is critical to understanding the biomolecular mechanisms for spider silk assembly and should have broad impacts on the biological materials community.

15. SUBJECT TERMS

16. SECURITY CLASSIFICATION OF:			**17. LIMITATION OF ABSTRACT**	**18. NUMBER OF PAGES**	**19a. NAME OF RESPONSIBLE PERSON**
a. REPORT	**b. ABSTRACT**	**c. THIS PAGE**			JUNG-HWA GIMM
U	U	U	UU	26	**19b. TELEPHONE NUMBER** *(Include area code)* 426-9542

1. Cover Sheet:

To: technicalreports@afosr.af.mil
Subject: Annual Performance Report to Dr. J. Aura Gimm

Contract/Grant Title: "The Molecular Mechanisms Responsible for the Assembly of Spider Silk Fibers"

PI: Gregory P. Holland

Institution: Department of Chemistry and Biochemistry, San Diego State University, San Diego CA 92182-1030

Contract/Grant #: FA9550-17-1-0282

Reporting Period: 1 June 2017 to 31 May 2020

2. Objectives (taken directly from the original proposal):

Spider's produce up to seven different types of silk that vary in mechanical properties from tougher than Kevlar to the extensibility of rubber and have the potential for numerous DOD applications ranging from high performance textiles to vehicle tires. However, because of the cannibalistic nature of spiders and the small amount of material produced compared to silkworms, scientists must manufacture the fiber in large quantities, and this requires that spider silk be produced with recombinant protein expression. With the advent of DNA sequencing for numerous spider silks and the recombinant expression of these sequences in various host organisms, researchers have moved one step closer to this end goal. The difficulty then arises when attempting to spin fibers from the recombinant silk protein dopes where the fibers produced do not match the superior mechanical properties of native spider silks. This is primarily due to differences in the folded structures of the silk proteins that comprise the fiber and ultimately, an inability to produce a spinning dope that behaves like native spider silk gland fluid. Hence, the ability to reproduce spider silk fibers in the laboratory is hindered by an incomplete molecular-level understanding of the native dope and the important biochemical triggers responsible for spider silk assembly. The objective of the proposed research is to build on results from our previous AFOSR funded research (Award No. FA9550-16-1-0151) and continue to explore the molecular mechanisms and biochemistry of the spider silk producing process. Our primary focus is to characterize the structure and dynamics of the protein-rich fluid in the various spider silk producing glands. There is surmounting evidence that the silk proteins organize into oligomeric assemblies in the silk gland and this feature could be critical for spider silk spinning. In addition to interrogating the spider silk dope, we have succeeded in growing spider silk fibers with dimensionalities and protein secondary structures that are approaching native spider silks. The resulting fibers grown directly from the native spider silk dope have assembly kinetics and structural features that depend on the biochemical conditions under which they were produced. The proposed study aims to continue this work by applying a combination of techniques to interrogate the various spider silk glands and fibers grown from the gland fluid including solution, solid-state and diffusion based nuclear magnetic resonance (NMR) spectroscopies in conjunction with cryo-electron microscopy (cryo-EM) and X-ray Diffraction (XRD). A list of specific aims that we hope to achieve in the proposed research is given below:

- Conduct three-dimensional (3D) protein solution NMR for native spider silk proteins as a function of pH and in the presence of various cations (Na^+, K^+) and anions (Cl^-, PO_4^{-3}). Determine with 3D protein solution NMR if these different biochemical conditions promote aggregation, impact protein folding, molecular structure and/or backbone dynamics (flexibility).
- Use pulse field gradient (PFG) Diffusion NMR to measure silk protein diffusion coefficients and overall transport properties. Determine the extent of silk protein entanglement and oligomerization at native spider gland conditions and as a function of protein concentration, pH and in the presence of various cations and anions.
- Conduct cryo-EM experiments to image silk proteins and determine the extent of oligomerization. Determine the size, shape and overall dimensionality of silk protein

oligomers at native conditions and following incubation in different denaturants (e.g. Urea and guanidinium chloride). Compare cryo-EM results with PFG NMR diffusion data.

- ✦ Utilize and develop modern multinuclear, multidimensional magic angle spinning (MAS) solid-state (SS)NMR techniques to structurally characterize spider silk fibers grown from the gland fluid in various ways including acidification and variability in salt concentrations. Establish the relevant processing conditions for converting the gland fluids to a fibrous material with structural features that match native spider silk fibers.
- ✦ Perform X-ray diffraction (XRD) measurements on silk fibers grown from the gland fluid under the above stated conditions to characterize molecular and hierarchical structures formed in these materials. XRD will focus on pair-distribution functional (PDF) analysis for characterizing amorphous structures and distributions as well as a combination of wide and small angle x-ray scattering (WAXS and SAXS) for characterizing structures in the 1-100 nanometer length scale.

3.1 Status of Effort (Year 1):

The primary objective of the proposed research is to elucidate the interactions, mechanisms and biochemistry of the spider silk producing process at the molecular and nanoscale levels. Our primary focus is to characterize the protein-rich fluid in the various spider silk producing glands. We have been using a variety of NMR methods including solution, diffusion and solid-state techniques together with cryo-EM and WAXD and SAXD at Argonne National Laboratory (ANL) to probe silk protein structure and dynamics prior to and following fiber formation. A combination of diffusion NMR and cryo-EM were used in year one to illuminate the supramolecular organization of silk proteins in the gland environment, a characteristic that should be critical to the development of robust spinning dopes that behave like native ones (*PNAS,* **2018**).[1] We have established a number of methods for isotopically ($^{2}H/^{13}C/^{15}N$) enriching the silk proteins during the course of our AFOSR funding that have allowed us to investigate native spider silk proteins within the silk gland and in the final spun fiber. We have used these isotope labeling approaches and SSNMR to elucidate the conformational structure of a relatively unexplored spider silk that is used to wrap prey and as the inner linings of egg cases (*Chem. Commun.,* **2018**).[2] Investigations on silks from different organisms including silkworms have continued in year one to understand the structure-function relationship in silks from various species and organisms (*Biomacromolecules,* **2018**).[3] Our research team has continued to develop magnetic resonance imaging (MRI) methods to probe the silk producing process *in vivo* (*Nature Review Materials*, **2018**).[4] Lastly, we recently published a review article on state-of-the-art experimental methods for characterizing the secondary structure and thermal properties of silk proteins in collaboration with the Kaplan Lab (*Macromol*. *Rapid Commun*., **2018**).[5]

4.1 Accomplishments/New Findings (Year 1):

Our research team has made considerable progress in understanding the supramolecular organization of spider silk proteins in the major ampullate (MA) silk gland during year 1 funding. Many natural silks produced by spiders and insects are unique materials in their exceptional toughness and tensile strength, while being

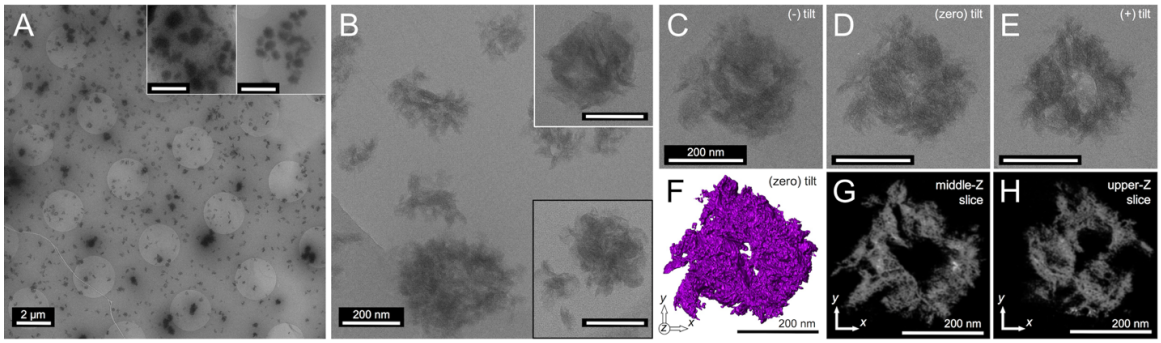

Figure 1. Native *L. hesperus* MA silk protein imaged by cryo-TEM (4 hr incubation in 4M urea). (*A*) Low-magnification image showing abundance of generally spherical (200-400 nm) micellar protein assemblies. Insets (2 µm scale bar) highlight the small population of the largest assemblies found (~500-800 nm). (*B*) High-magnification images of the spidroin hierarchical assemblies, representative of the highest populations; spherical micellar assemblies composed of disordered "flake-like" sub-domains (200 nm scale bar for insets). Black boxed inset shows similar structures found in a sample prepared from a separate spider following the same procedure. (*C-E*) Cryo-TEM images from a tomography tilt-series of one selected hierarchical protein nano-assembly. (*F*) 3D isosurface rendering of the assembly in *C-E*. (*G,H*) ~0.8 nm thick z-slices extracted at different *z*-heights from the tomography reconstruction in *F* of the assembly in *C-E*.

lightweight and biodegradable; properties that are currently unparalleled in synthetic materials. A number of approaches have been attempted to prepare artificial silks from recombinant spider silk spidroins but, have each failed to achieve the advantageous properties of the natural material. We believe that this is because of an incomplete understanding of the *in vivo* spidroin-to-fiber spinning process and particularly, because of a lack of knowledge of the true morphological nature of spidroin nanostructures in the precursor dope solution and the mechanisms by which these nanostructures transform into micron-scale silk fibers. Very recently, we determine the physical form of the natural spidroin precursor nanostructures stored within spider glands that seed the formation of their silks and revealed the fundamental structural transformations that occur during the initial stages of extrusion *en route* to fiber formation. Using a combination of solution phase diffusion nuclear magnetic resonance (NMR) and cryogenic transmission electron microscopy (cryo-TEM) we revealed direct evidence that the concentrated spidroin proteins are stored in the silk glands of Black Widow spiders as complex, hierarchical nano-assemblies (~300 nm diameter) that are composed of micellar subdomains, sub-structures which themselves are engaged in the initial nanoscale transformations that occur in response to shear (**See Figure 1**).[1] We found that the previous established micelle theory of silk fiber precursor storage is incomplete, and that the first steps towards liquid crystalline organization during silk spinning involve the fibrillization of nanoscale hierarchical micelle sub-domains. In this work we showed that larger, hierarchical micellar nano-assemblies are the initial protein structures in the native dope; the seeds from which natural silk fibers are spun. Achieving similar synthetically produced hierarchical nano-assemblies (several hundred nanometers in diameter) will be critical for bulk-producing robust synthetic silk fibers from recombinant spidroin proteins. For more on this work see reference 1.

During year one of funding we began exploring a relatively unexplored spider silk called aciniform (AC) silk that is used for wrapping prey and lining egg cases. Spiders produce up to seven different types of protein-based structural materials including six types of silk that have a range of mechanical properties from rubber extensibility to

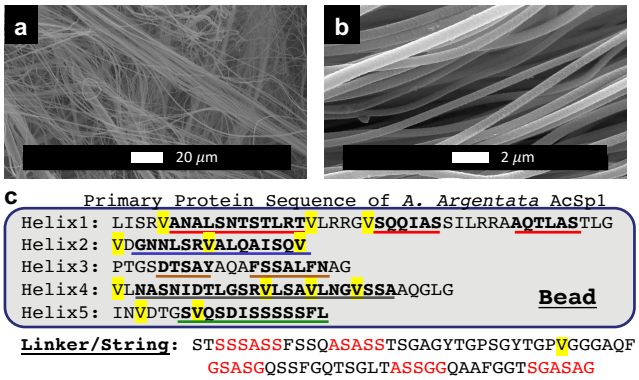

Figure 2. Scanning Electron Microscopy (SEM) images (a, b) of native *A. argentata* prey-wrapping silks. Fibers are roughly 500 nm in diameter. (c) Primary-protein sequence for *A. argentata* AcSp1 repeat unit. Regions determined to be helical in solution are bolded and color-underlined based on structure homology between *A. trifaciata* (PDB Code 2MU3) and *A. argentata*. Val residues are highlighted in yellow and proposed β-sheet-forming motifs from the linker region are shown with red lettering.

Kevlar-like toughness and a glue-like adhesive substance. To date, the vast majority of structural data on as-spun silk fibers has been on MA silks due to their unmatched strength and ease of collection and study. However, through a unique combination of high strength (~700 MPa) and high extensibility before breaking (~60-80%) AC silk is actually the toughest of the spider silks and boasts mechanical properties that surpass the toughest man-made materials. A complete molecular-level understanding of native aciniform silk fiber is lacking (the origin of the unique mechanical properties), although significant insight into its protein structure can be gained from the current consensus model for spider dragline fibers and from solution phase NMR work conducted on recombinant aciniform spidroin 1 (AcSp1) protein.

The high strength and moderate extensibility of dragline fibers is largely attributed to common structural motifs arising from short repetitive protein units; high fiber strength is thought to arise from aligned nanocrystalline β-sheet domains comprised of a poly(Ala) and poly(Gly-Ala) and sometimes Ser, while Gly-Gly-X and Gly-Pro-Gly-X-X repeats contribute to fiber extensibility in the form of randomly-oriented domains and elastin-like type II β-turns. On the other hand, the consensus sequence of AcSp1 is composed of a string of ~14 much longer repeats of about 200 amino acids, flanked by non-repetitive C- and N-terminal regions. The AcSp1 sequence contains both Ser-rich and Ala-Ser rich motifs (**Figure 2c**, red lettering), but AC silks are entirely deficient in the traditional poly(Ala), poly(Gly-Ala), Gly-Gly-X and Gly-Pro-Gly-X-X repeats found in dragline spider silks. It was assumed through crude sequence-based structure predictions that AcSp1 repeats are likely to be rich in α-helices and this assumption was confirmed when the complete liquids NMR structure of the *A. trifaciata* AcSp1 wrapping unit was solved (PDB code 2MU3), where the AcSp1 protein exists as a multi-domain "beads on a string" structure composed of a well-defined 5-helix globular domain (bead, helices 1-5) and a disordered linker domain (string) in solution.

To gain a more detailed view into the molecular structure of native prey-wrap silk fibers we utilized MAS SSNMR techniques. *A. argentata* and *A. aurantia* spiders were fed ~50 microliters of a saturated solution containing A) ^{13}C-labelled Ala (Ser is also labelled through metabolism of Ala), and/or B) ^{13}C-labelled Val every few days. Prey-wrap silk was collected by simulating prey using vibrating tweezers or a vibrating electric toothbrush. These labelling schemes were chosen to highlight the two distinct domains found in the aciniform repeat sequence (**Figure 2c**); namely that Ala and Ser are found dispersed throughout both the globular helical domain and the disordered linker region, while Val (and other hydrophobic residues) are found almost exclusively in the helical

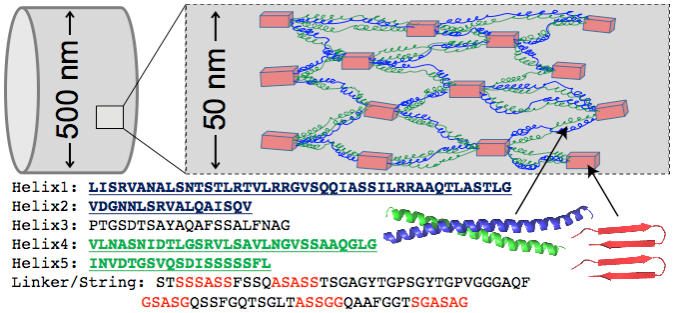

Figure 3. Proposed hierarchical molecular protein structure of AC prey-wrapping silks as a hybrid coiled-coil and nanocrystalline β-sheet fibroin. Helix 1 and 2 form a helical coil (blue), Helix 3 is unstructured, acting as a possible turn, helices 4 and 5 form another single coil (green), and the Ser / Ala-rich regions of the linker form pleated β-sheet (red) domains in the spun fiber.

globular region (bead); notably in helices 1, 2, 4 and 5 but none found in helix 3 and only two found in the linker. By utilizing advanced multi-dimensional MAS SSNMR data we were able to illustrate that prey-wrapping silks, which are actually the toughest biopolymer known, are dominated by α-helical secondary structures (~40-50% of total fiber) with only minor β-sheet content (15% total). We found that α-helix-to-β-sheet conversion is minimal upon fiber formation, and prey-wrapping silk β-sheet content is low compared to other spider silks. Spectral deconvolutions of NMR data show that β-sheet nucleation indeed occurs during fibrillization, but this is likely from Ser- and Ala-rich domains found in the linker region while the helical domains remain largely intact. We propose a hierarchical silk protein organization where the nanofiber is a hybrid α-helical coiled-coil assembly with a minor population of β-sheet domains (see **Figure 3**). True α-helical silks are observed in other insect silks (hornets, bees and wasps), but never before have they been observed in spider silks. AC silks are capable of extending about twice as far before breaking compared to dragline spider silk fibers, a unique mechanical property that is almost certainly a direct result of their high α-helical content. For more on this work see reference 2.

Our research team published a review article in collaboration with the Kaplan Lab at Tufts where we compiled and assessed the instrumentation techniques available for characterizing both the secondary structure and thermal properties of silk protein-based materials from both silkworms and spiders. The table of contents graphic summarizes this review and is shown in Figure 4. The secondary structure of silk proteins is a critical feature that determines the mechanical properties and stability of silk-based materials. In this review experimental techniques - both established methods and recent advancements - used for studying silk secondary structure, the information attainable from these

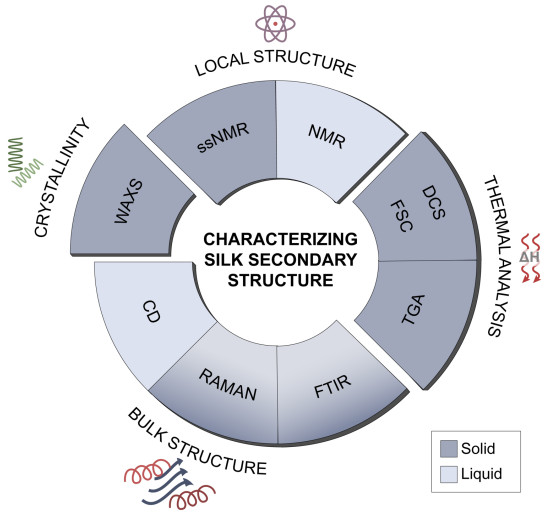

Figure 4. Silk secondary structure can be obtained from a range of methods including XRD, solution NMR, SSNMR, Raman, FTIR, WAXD and CD. The method chosen depends on the sample format (solid or liquid). These methods can provide in combination information regarding local structure, bulk structure and crystallinity. Thermal methods (DSC, TGA) can provide information regarding the silk thermal properties and some cases indirect information regarding secondary structure can be obtained

techniques, and their limitations were discussed. Ultimately, successful structural characterization will require a combination of the methods reviewed here. It is important to note that site-specific atomic level structure can only be obtained from solution and solid-state NMR for the dope and solid materials (fibers, films, ertc), respectively. Raman and FTIR can be used to obtain some information about secondary structure such as the β-sheet fraction but, quantification is still a challenge. X-ray techniques can be used to determine crystallinity and is best when used in combination with solid-state NMR to obtain amino-acid-specific information when investigate fibrous silk materials. CD can provide some information regarding structuring in the dope spinning fluid while, thermal analysis methods (TGA, DSC, FSC) can provide information about the thermal properties of the materials where some information regarding protein secondary structure can be obtained indirectly from heat flow information such as transition temperatures and enthalpies. For more on this review see reference 3.

In a second review article our research team published a *Nature Reviews Materials* article on uncovering the structure function relationship in spider silk. This article provided an overview of the experimental and computational studies that have provided a wealth of detail at the molecular level on the highly conserved repetitive core and the termini of spider dragline silk proteins. The role of the nanocrystalline b-sheet regions and amorphous regions in determining the properties of spider silk fibers, imparting them with high strength and modest extensibility which in combination make it one of the toughest materials known. Imaging techniques including magnetic resonance imaging (MRI) and modeling studies illustrate the importance of the hierarchical structure and organization of the proteins that comprise the silk fibers. The hope is that these insights into structure-function relationship can guide the reverse engineering of spider silk to enable the production of superior fibers. An example of MRI imaging of the silk spinning system within a Black Widow spider's abdomen is shown in Figure 5. We

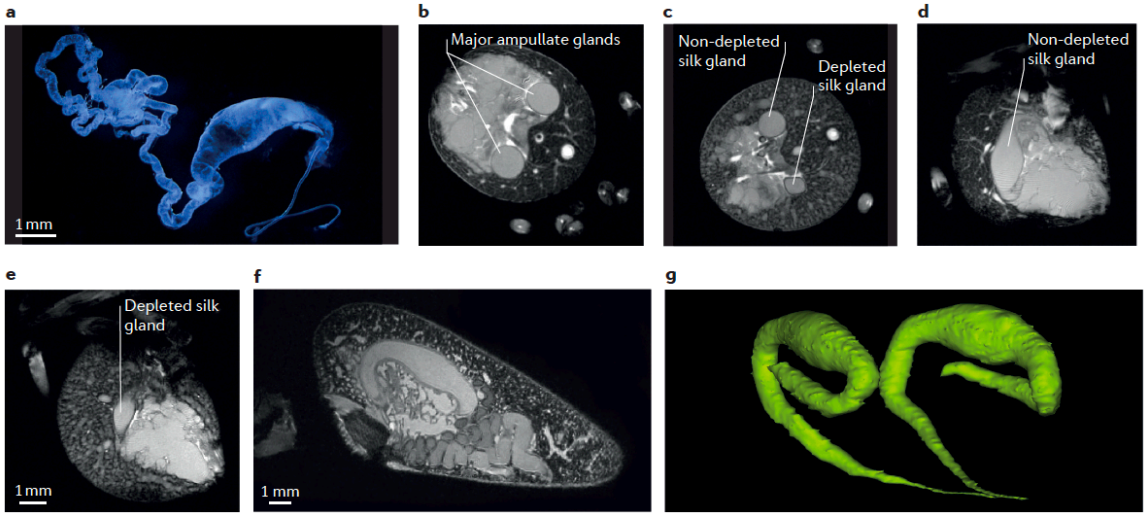

Figure 5. The major ampullate glands. (a) A dissected major ampullate gland from the black widow (*Latrodctus hesperus*) spider. (b-e) MRI images collected at 18.8 T from a live black widow spider before and after pulling silk from the major ampullate glands. The in-plane resolution is 46 μm x 46 μm and the in-plane thickness is 300 μm. (f) A slice from an 18.8 T 3D MRI image of the abdomen of a golden orb weaving spider (*Nephila clavipes*) with an isotropic resolution 39 μm. (g) The corresponding 3D surface of the major ampullate glands. The gland volume, including the portion of the tail and duct measures 8.5 μL.

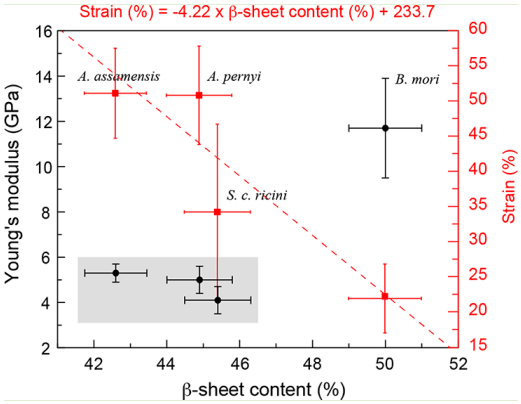

Figure 6. Mechanical properties (Young's Modulus and Strain) plotted as a function β-sheet content for degummed silkworm silks collected from different species of silkworm. The β-sheet content was determined using a combination of spectroscopic (IR, SSNMR) and XRD methods. A strong correlation between mechanical properties and silk protein β-sheet secondary structure is observed.

are currently working to couple this approach with NMR spectroscopy to interrogate the spinning process at the molecular level while, imaging along the silk gland and duct. It is anticipated that as this approach is further developed that we will be able to provide an unprecedented level of detail and insight into spider silk spinning. For more on this work see reference 4.

We continue to explore the silks from other silk producing organisms including silkworms and recently illustrated that the β-sheet fraction determined from a suite of spectroscopy (FTIR, SSNMR) and X-ray diffraction approaches directly correlated with a number of the silk's mechanical properties.[5] Silkworm silk has attracted considerable attention as a biomaterial due to its excellent mechanical properties, biocapatibility and biodegradability. However, a clear understanding of how the underlying molecular structural features such as the impact of secondary structure on the fiber mechanical properties is still lacking. In a recent study our team conducted a thorough comparative structural analysis of degummed silk fibers from four silkworm species (*B. Mori, A. pernyi, S.c. ricini* and *A. assamensis*). A summary of these results is displayed in Figure 4 and illustrate the strong dependence of the mechanical properties on the fraction of β-sheet secondary structure in the silk fiber. Specifically, we have found that the strength as defined by the Young's modulus increases with the β-sheet fraction while, the strain shows a linear decrease with β-sheet content. Thus, silk fibers with high β-sheet content will tend to be stronger but, less extensible. This shows how we can use a combination of spectroscopic methods and mechanical testing to correlate structure-function in silk fibers. We are now in the process of extending these methods to characterize the influence of the other secondary structures (random coil, β-turn and helical) on mechanical properties and extending these approaches to MA spider silks from different species of spider and the various types of spider silk. For more on this work see reference 5.

5.1 Status of Effort (Year 2 & 3):

In years 2 and 3 we continued to investigate prey wrap spider silk and the structure and dynamics of the silk protein within the spider silk producing MA gland using a variety of solution NMR methods, DLS and mechanical dynamics (MD) simulations. NMR permits the characterization of the atomic and molecular level interactions that facilitate the assembly of the supramolecular (200-300 nm diameters, ~300 proteins) micelles observed by cryo-TEM and diffusion NMR (see reference 1). For prey wrap spider silk we have focused on the interaction with water where we have found that as spun fibers are individual 500 nm fibers but, after exposure to water the fibers

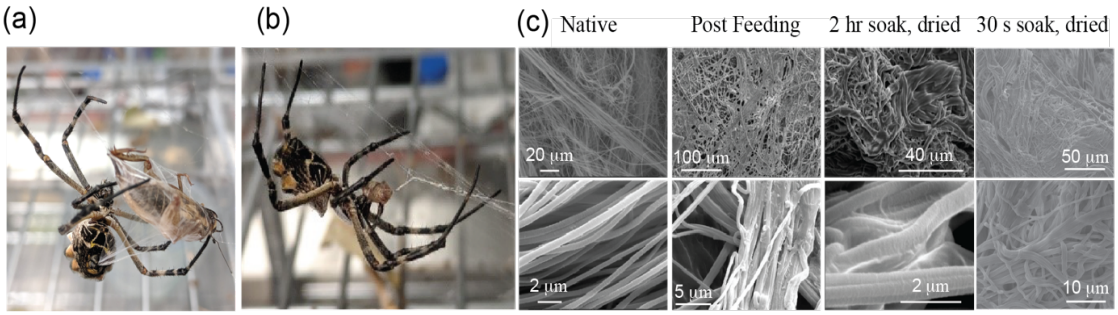

Figure 7. a), *A. argentata* spinning a cricket with AC silk. b), the same spider returning to eat its prey through EOD. c), SEM images comparing native prey-wrapping AC silk from *A. argentata* following feeding or water treatment where the silk was soaked for 2 hr or 30 s and then dried for one day.

cross-link and change from being extensible and flexible to a stiff matted morphology (see reference 9). The results of this efforts are detailed below.

5.2 Accomplishments/New Findings (Year 2 & 3):

Due to its moderate strength (~700 MPa) and impressive extensibility before breaking (~60-80%), orb-weaving spider AC prey-wrapping silks are actually the toughest of the spider silks but are remarkably understudied. Our previous results indicate that native AC silk fibers are an α-helix rich coiled-coil / β-sheet hybrid nanofiber, and that conversion of disordered or helical domains to β-sheet aggregates is surprisingly minimal and overall β-sheet content is low (~15%) (Figures 2 and 3 above, and reference 2). In this effort, we demonstrate through Scanning Electron Microscopy (SEM) that native AC silk fibers undergo matted cross-linking upon exposure to moisture that increases silk stiffness as judged by nanoindentation experiments (data not shown). The unique molecular mechanism of water-induced cross-linking is revealed SSNMR) methods; water-induced morphological changes are correlated with an increase in AC silk protein β-sheet content, and additionally we observe a minor unfolding of coiled-coil regions. Continued and increased β -sheet cross-linking is observed upon application of mechanical shear. We determine the size of these β-sheet domains to be 4-6 nm using WIdeline SEparation (WISE) SSNMR. The observation that merely water treatment can be used to convert a protein-based material from a flexible/extensible α-helix-rich fiber to a rigid crossed-linked β-sheet mat is a novel observation that should provide new avenues in bioinspired materials design.

Freshly-collected AC silk is shown as a dense mesh of fine (~500 nm in diameter) fibers (Figure 7c). When we attempted to image silk on a wrapped and consumed prey (cricket), we were surprised to observe clear morphological changes to regions of the silk. Dense bundles of individual AC fibers remain, but areas of wrapping silk fibers appear to have fused together into fibrous sheets or mats, especially in regions where the silk makes direct contact with the cricket. Additionally, inter-fiber space appears to have collapsed. To determine the effect of water on AC fiber morphology, native prey-wrapping silk was briefly soaked in deionized water for two hours without mechanical agitation and dried for 1 day. SEM images of our water-wetted silk bundles confirm that this observed cross-linking property is water-induced. The effect of hydration on silk structure has been investigated for several silk-based materials including native silk fibers, recombinant silk protein films, and peptides. The effect of water on protein secondary structure has been conclusive, and results in an increase in β-sheet content of

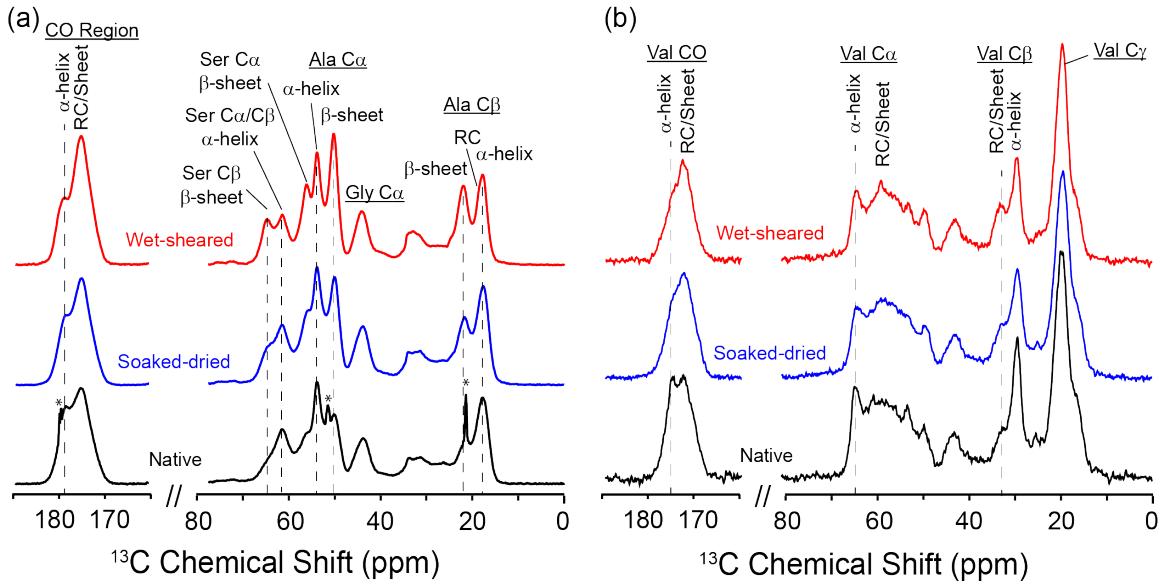

Figure 8. ^{13}C CP-MAS SSNMR spectra of *A. argentata* AC silk. a) AC silk labeled with ^{13}C-Ala. b) AC silk labeled with ^{13}C-Val. Peaks in a) with asterisks are from crystalline Ala contamination.

the materials, including silkworm silk fibers. However, these changes occur within a single fiber, not between adjacent strands. After allowing our AC silk fibers to air-dry, the material became noticeably stiffer and was no longer malleable like the native silk fiber. It is possible that other factors, such as dissolved salts and pH used in the native (wrapped cricket) fibers, may fine tune the local silk fusion and aggregation to minimize fluid loss from the prey. The appearance of nearly identical morphological structures in both native and water-treated samples, however, leads us to the conclusion that AC silk protein-water interactions drive the mechanism for fiber fusion and cross-linking. Lastly, the fiber fusion and cross-linking process occurs rapidly with similar observations made for AC silks water treated for 2 hr and 30 s (Figure 2c).

To better understand the structural changes induced by both moisture and mechanical agitation, SSNMR data was collected on AC silks after two types of sequential treatment. After initial SSNMR analysis on the native fibers (Native, **Figure 8**, black), the AC silk was removed from the NMR rotor and soaked with DI water at room temperature for two hours without any mechanical agitation and allowed to air-dry ("Soaked- dried", Figure 8, blue). After data collection, the AC silk was re-hydrated and loaded into the rotor while still wet which allows the spinning rotor to induce physical shear, removed and dried for two days, then reloaded. ("Wet-sheared, dried", Figure 8 red). The changes to the protein secondary structure for several amino acids found throughout the W subunit were monitored throughout this process.

Several conclusions can be drawn from comparing 1D ^{1}H/^{13}C cross polarization magic angle spinning (CP-MAS) spectra between the native and water-treated AC silk (Figure 8a). When scaling the 1D ^{13}C-Ala-labeled CP-MAS spectra based on the Gly Cα resonance, it becomes clear that Ala β-sheet content increases moderately upon water wetting (Figure 8a). The reader is reminded that this sample was only submerged in water for two hours with no agitation and allowed to air-dry prior to data collection, thus these structural changes are truly a result of exposure to water and not from shearing or

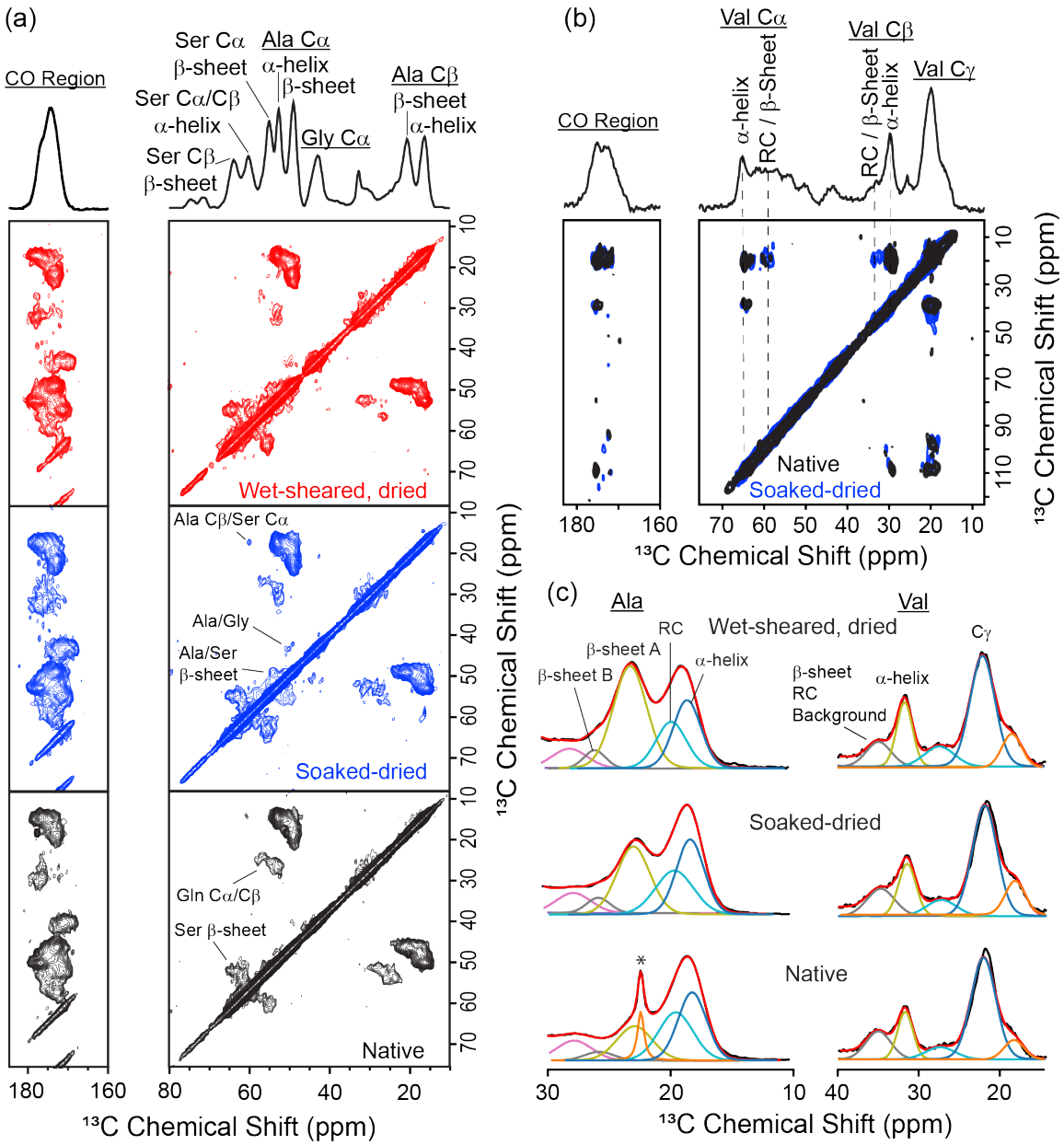

Figure 9. a), 2D ^{13}C-^{13}C DARR SSNMR spectra collected with a 100 ms mixing time for ^{13}C-Ala-labeled *A. argentata* AC silk after different treatments. b), the same as in a) but only ^{13}C-Val labeled. c), spectral deconvolutions of 1D ^{13}C CP-MAS data showing qualitative changes to the Ala Cβ (left) and Val Cβ (right) resonance after different treatments.

mechanical stress caused by MAS. It is not immediately clear if this observed structural transition is due to unfolding of α-helical environments in favor of β-sheets, or if previously disordered regions of the silk protein are enticed to aggregate. Insight is gained through spectral deconvolutions of the data. To understand water-induced arrangements that have been proposed from studies on silk-like model peptides. This procedure is well outlined in the supplemental section of reference 2 and was applied here. These results show that the β-sheet content for Ala increases from ~30% for the

native silk to ~41% following hydration and reaches a maximum of ~53% after wet-shear and drying (Figure 9). As a comparison, Ala within poly(Ala)-rich spider dragline silks show much higher β-sheet content at 82%. This increase in β-sheet content for AC silks is mirrored by a decrease of Ala in RC structures, followed by α-helical structures after shear. Ala occupies α-helical, RC and β-sheet structures in approximately equal proportions after wetting. After wet-shearing and drying, Ala adopting α-helical and RC structures further decreases while β-sheet content increases to nearly half. The solution structure of the W subunit shows that helix 1 contains 11 of the 26 Ala residues, where the linker contains five. Therefore, this data implies Ala conversion likely comes from the partially-coiled helix 1 and linker regions (see reference 2 and 9 for sequence information).

Similar to Ala, there is a clear but minor increase in Ser adopting β-sheet structures after exposure to water. The relative intensity of the Ser Cα and Cβ β-sheet resonances at 55 and 65 ppm increase slightly upon exposure to water, and then increase dramatically after wet-shearing (Figure 8a). In our previous model of native AC silks Figure 3), we demonstrated that the poly(Ser) motif at the end of helix 5 remains helical in the final fiber (reference 2). This is intriguing, since poly(Ser) motifs found in other insect silks have been shown to form β-sheet structures. While a partial α to β conversion of this poly(Ser) helix 5 may occur during water-wetting, the surprisingly low conversion towards β-sheets with only soaking suggests that a full conversion does not occur. After wet-shearing and drying, we see a more substantial decrease in Ser α-helix content in favor of β-sheet structures, implying collapse of the poly(Ser) helical motif.

1D ^{13}C CP-MAS data for ^{13}C-Val enriched AC silk before and after water-wetting suggests that Val helical structures partially collapse from 62% to ~51% (Figure 9c) where broad and weak Val Cα/Cγ and Val Cβ/Cγ cross-peaks in the 2D DARR become slightly stronger (Figure 9b). This qualitative observation is supported by spectral deconvolutions of the Val Cβ signal, although we could not confidently separate β-sheet and RC structures (Figure 9c). Since Val residues are almost exclusively found in the globular "bead" region and adopt coiled-coil like superstructures in the final fiber, it is likely that a minor conversion of Val from helical to RC and/or β-sheet motifs occurs in this region upon exposure to water. One explanation for this conversion is that several of the Val residues in the "bead" region are found as Gly-Val/Val-Gly pairs. Perhaps the juxtaposition of Gly and Val create a more favorable RC or β-sheet environment during water-wetting, since Gly is known to be unstructured in many proteins. Indeed, closer inspection of the Gly peak in the Ala-labeled native AC silk (Figure 8, 9) shows a shoulder at ~47 ppm, corresponding to Gly in an helical environment, which decreases after treatment with water and suggests Val in Gly/Val pairs are no longer α-helical.

After wet-shearing and drying, a slight collapse in helices occurs from 54% to ~51% favoring RC and/or β-sheets, however the predominant structure for Val still remains α-helical. This observation strengthens our prior conclusion that Val residues predominantly exist in well-folded highly-stable α-helical coiled-coil hierarchical structures within spider prey-wrapping silks and conversion to β-sheet due to wetting or wet-shearing is minimal. The high degree of order for Val in α-helical coiled-coil assemblies is further supported by the linewidth of the Val Cβ resonances that are

considerably narrower (285 Hz) compared to all other Cβ amino acid linewidths (315-510 Hz) in other structures.

2.3 β-sheet Domain Sizes in AC Silk

Since β-sheet formation is the dominant underpinning behind hydration-induced cross-linking of prey-wrapping silk, we next implemented the 2D WIde-Line SEparation (WISE) NMR technique with ^{1}H spin-diffusion to elucidate the domain size and overall water-accessibility of these β-sheet nanostructures. The concept behind the technique is outlined in reference 9, but briefly, by observing the ^{13}C chemical shift in the direct dimension and measuring the associated ^{1}H profile in the indirect dimension, the 2D WISE NMR technique is capable of correlating local biopolymer conformational structure with mobility and dynamics. A 1D ^{1}H slice is typically extracted from the 2D ^{1}H/^{13}C WISE SSNMR spectrum to reveal the ^{1}H lineshape at a specific ^{13}C chemical shift where broad ^{1}H lineshapes are associated with “rigid” ^{1}H environments, while narrow ^{1}H profiles would arise from more "mobile" regions.

Importantly, if a ^{1}H spin-diffusion period is included in the WISE experiment it is possible to observe magnetization from the "mobile" water-plasticized regions diffuse into these water-inaccessible domains which ultimately allows for domain-size to be determined for the rigid domains. In this study we applied the WISE technique to both Black Widow (BW) dragline silk fibers and cross-linked AC silks and compared the

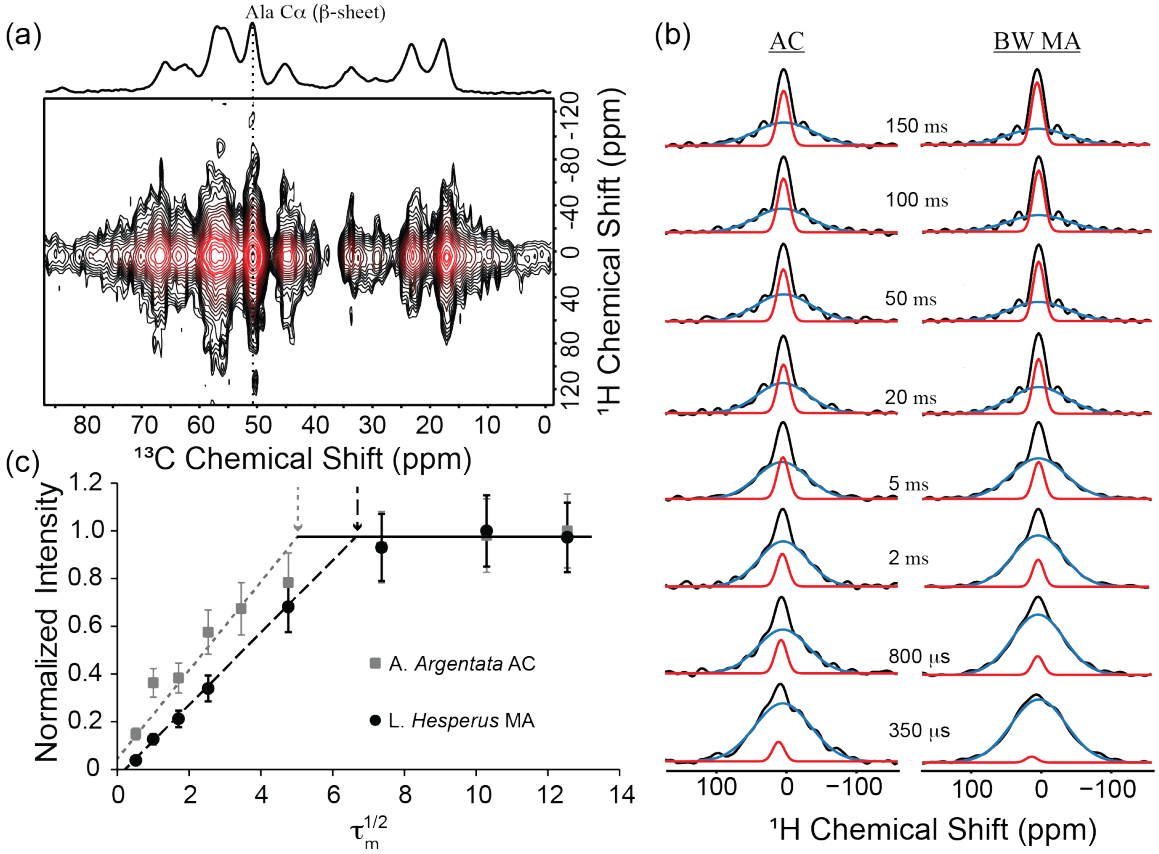

Figure 10. (**a**) A 2D ^{1}H/^{13}C WISE spectrum with a 50 ms spin-diffusion time for hydrated *A. argentata* AC silk. (**b**), deconvoluted fits of ^{1}H slices extracted at the Ala Cα β-sheet resonance in the WISE spectrum for AC silk and BW dragline. (**c**), build-up curves of narrow component (red) from deconvolutions for the two silks. The arrows indicate τ_m^* for each sample.

respective β-sheet domain sizes and overall fiber rigidity. The extracted ^{1}H profiles were fit to both broad and narrow components for each mixing time, and the area of the narrow component was plotted against the square root of the spin-diffusion mixing time (see Figure 10). The point (τ_m^*) at which the narrow component reaches a plateau implies that diffusion of magnetization from the "mobile" domain into the "rigid" domain has reached an equilibrium. Larger domains would require more time to reach equilibrium.

WISE experiments were collected on AC silk and BW dragline (MA) fibers using spin-diffusion times between 0.05-150 ms (Figure 10a). Slices were extracted from WISE experiments at the Ala Cα β-sheet resonance and fit to a broad and narrow component (Figure 10b). We found the following major conclusions from the WISE buildup data on cross-linked AC silk fibers; 1) a large fraction of Ala residues adopting β-sheet secondary structures within AC silks are inherently water accessible, 2) Gly residues are more dynamic within AC silks compared to BW dragline silks, and 3) water-inaccessible β-sheet nanodomains are significantly smaller in cross-linked AC silks compared to well-characterized BW spider dragline β-sheet nanocrystallites. Similarly, based on the high initial offset and quick rise to equilibrium, it is clear that Gly residues within AC silks are highly mobile even after water-induced crosslinking. Third, analysis of the Ala Cα spin-diffusion buildup curves for water-hydrated AC and BW dragline silks clearly indicate that the Ala-rich β-sheet domains in cross-linked AC silks are smaller than in BW dragline fibers. Using the previously-derived equation to calculate domain size, we determine the β-sheet domains in cross-linked AC silks to be between 4-6 nm (detail in supporting information of reference 9). Additionally, we calculated the size of the nanodomains in BW dragline silk to be approximately 11 nm, somewhat larger than reported by XRD results which show a crystallite size of 3.02 x 4.15 x 6.71 nm. The difference in size could be due to the well-diffracting, truly crystalline areas of these nanodomains which may be smaller than the water-inaccessible β-sheet domains we probe with NMR. Figure 11 shows a proposed model to illustrate the structural changes of AC silks after water treatment.

In summary, we have shown that prey-wrapping silks from the garden spider *A. argentata* undergo a remarkable cross-linking behavior when exposed to moisture that

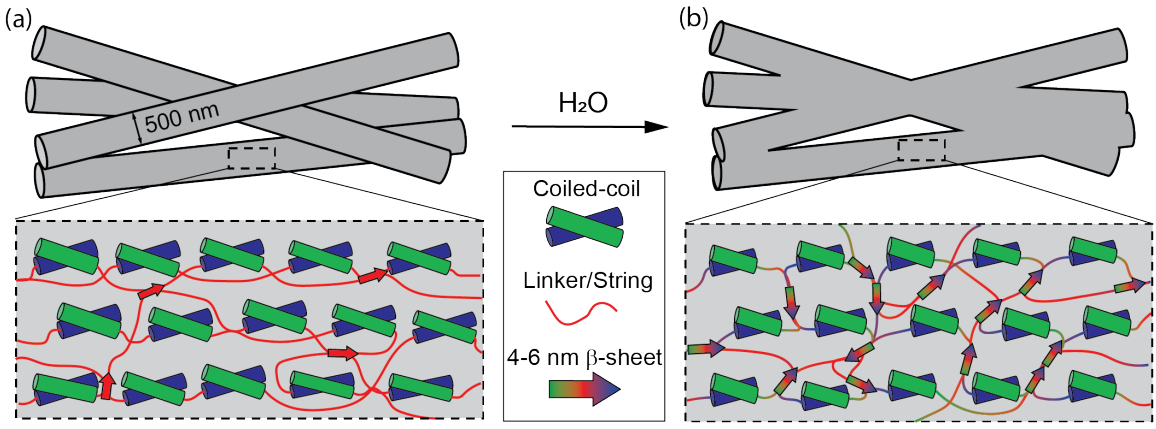

Figure 11. Proposed model of AC silks after contact with water. Helices 1-5 are blue and green cylinders that form α-helical coiled-coils. (**a**), before wetting there is little β-sheet content (~15%). (**b**), after water wetting some α-helical and RC structures convert to β-sheet, illustrated as shortened coiled-coils and the multi-colored arrows colored according to their origin from RC and/or helix structures.

has not been observed in other silks to the best of our knowledge. Upon contact with water, SEM images reveal that individual silk fibers fuse together to form cross-linked fibrous sheets and mats. Comprehensive solid-state NMR data on ^{13}C-enriched wrapping silks has uncovered the molecular mechanism of inter-fiber cross-linking. Orthogonal isotopic enrichment schemes (Ala-labeling and Val-labeling) were chosen to understand these structural changes for Ala, Ser, Gly, and Val residues, shedding light on which regions of the primary protein sequence are most susceptible to water-induced β-sheet crosslinking. Overall, the data reveals that water-induced fiber cross-linking is driven by an increase in β-sheet protein secondary structure at the expense of disordered and loosely-structured α-helical motifs, whereas well-ordered coiled-coil structures remain in-tact for the most part. However, helical coiled-coil motifs also undergo partial α-to-β conversion with the addition of mechanical shear. Finally, WISE NMR data was used to estimate the β-sheet domain sizes and overall protein dynamics within water-hydrated wrapping silks. Even after water-induced crosslinking, β-sheet regions within AC silks are smaller (~4-6 nm) than those found in BW dragline fibers (~11 nm), suggesting that newly-formed β-sheet structures are small in size and likely between two or more protein chains and potentially involving multiple fibers.

It is anticipated that the concept of utilizing water treatment to convert protein-based biomaterials from flexible and extensible, dominated by α-helical coiled-coil hierarchy, to rigid crossed-linked β-sheet assemblies, should provide new avenues in bioinspired material design. The potential for this hydration-induced conformational switching behavior in a biomaterial are hypothesized to impact a broad range DOD-AFOSR applications that all require ever evolving functional materials. In the defense sectors new novel materials based on the aciniform silk system could be utilized in advanced textiles for protective clothing, parachutes, delivery devices, arresting cables and the repairs of such materials.

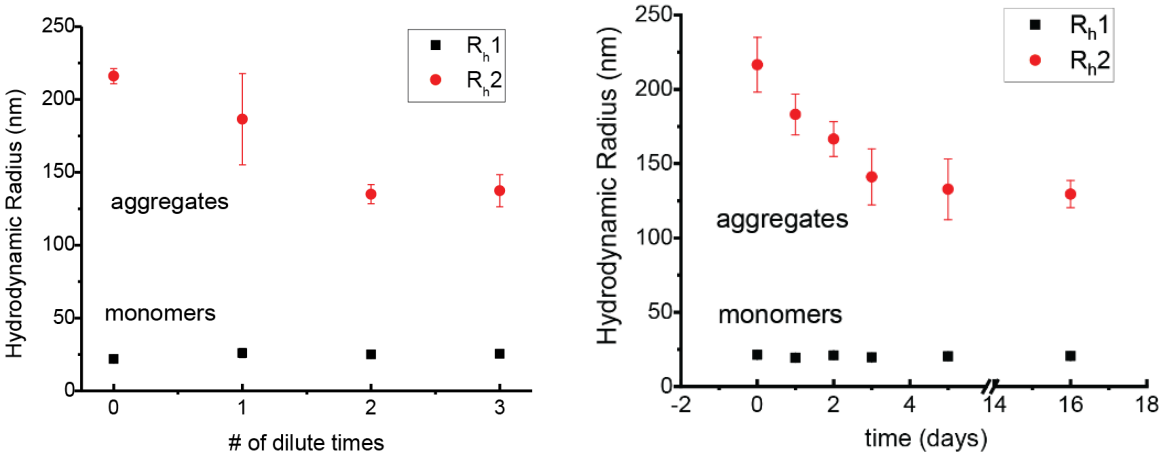

Figure 12 Hydrodynamic radii determined from DLS for native MA spidroins dissolved in 4M urea and measured as a function of concentration (Left) and time (Right). Both monomers and large protein assemblies (aggregates) are observed. A decrease in the size of the larger assemblies appears to stabilize after a few days. Monomer sizes remain roughly the same as a function of concentration and time. Dilutions correlate directly to the wt% values reported in Table 1, namely 0.1, 0.05, 0.025, 0.0013. The sample measured over time has a concentration of 0.1 wt%.

Table 1 Hydrodynamic radii determined from DLS for native MA silk proteins in 4M urea as a function of dilution. The smaller component around 22 nm agrees with NMR and empirical measures of the size of a single monomer of MaSp1. The larger component agrees, at least in general length scale, with the larger pre-assemblies previously observed by both diffusion NMR and Cryo-TEM. Both monomers and large protein assemblies are always observed with the superstructure decreasing in size with decreasing concentration.

Dilution Factor	D_1 (cm2/s)	R_{h1} (nm)	D_2 (cm2/s)	R_{h2} (nm)
0.100 %wt	(9.26 ± 0.88) E-8	22.0 ± 2.3	(9.42±0.22) E-9	216.0 ± 5.2
0.050 %wt	(7.81 ± 0.46) E-8	26.0 ± 3.1	(1.09±0.22) E-8	186.5 ± 31.3
0.025 %wt	(8.12 ± 0.13) E-8	25.1 ± 0.5	(1.51±0.07) E-8	135.0 ± 6.6
0.013 %wt	(8.02 ± 0.59) E-8	25.4 ± 2.1	(1.48±0.11) E-8	137.4 ± 11.0

Our research team has made considerable progress in understanding the structure of the silk spidroins and the intermolecular interactions that facilitate their supramolecular organization into pre-assemblies prior to fiber formation. Utilizing dynamic light scattering (DLS) one can measure the scattering of light by particles in solution and can be used to determine the hydrodynamic radii of individual protein monomers and larger superstructures comprised of 100's of spidroins. Previously, we illustrated with routine DLS, that dilute solutions of native MA spider silk dope dissolved in 4M urea contain both spidroin monomers (~19 nm) and larger protein assemblies with diameters on the order of 200-300 nm (reference 1). More recently, we used multi-angle DLS to track the size of these assemblies as a function of concentration and time (Figure 12, Table 1). DLS provides an excellent measure of the dynamics and size of the monomeric MA silk proteins and larger-scale spidroin assemblies and superstrcutures. Furthermore, DLS is extremely sensitive down to low protein concentrations, well below what can be observed with NMR. The large spidroin assembly decreases in size as a function of both time and concentration (Figure 12, Table 1**).** Stability is reached after a few days, which suggests that some fraction of the larger assemblies is long lived however, they decrease in size with decreasing concentration and increasing time.

In order to get a better handle on the atomic-level intermolecular interactions that are responsible for the spidroin superstructures solution NMR was used. We know from the DLS measurements that the spidroin micelle superstructures decrease in size as a function of decreasing concentration and increasing time in 4M urea. We now aim to interrogate the intermolecular interactions between spidroins that facilitate the large MA micellar superstructures. By conducting NMR experiments at different concentrations and times in 4M urea, perturbations in NMR observables (isotropic chemical shifts, relaxation times) are attributed to the disassembly of the large spidroin superstructures. In the $^{1}H/^{15}N$-HSQC, we observe 12 resonances which correspond to three separate regions: Gly-rich, Gln-rich and Ala-rich (Figure 13). These same twelve resonances have been observed in solution NMR spectra of intact glands previously and we are able to directly compare the two sets of resonances. Similar to intact glands, very narrow chemical shift (~0.5 ppm) dispersion in the ^{1}H dimension is observed indicating unstructured, highly

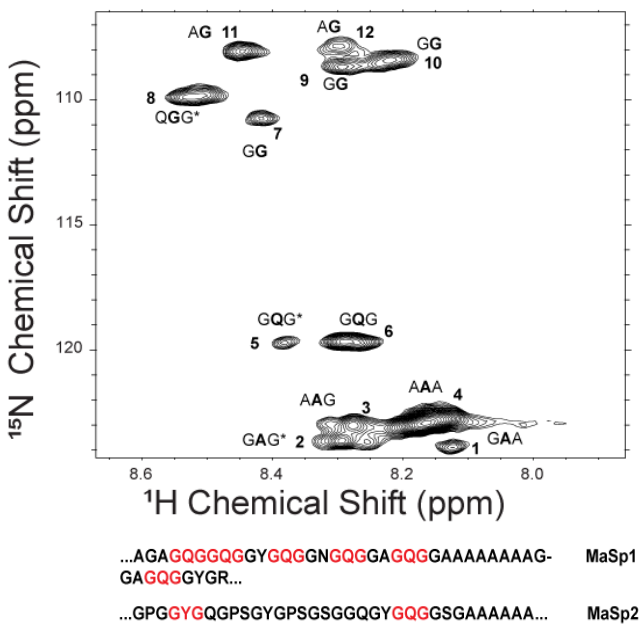

Figure 13. $^{1}H/^{15}N$-HSQC with 12 regions assigned for MA silk gland proteins dissolved in 4M urea. The triple residue assignments were determined from the 3D spectra shown in Figure 9. An example of the repetitive core regions of both MA spidroins is shown below the spectrum illustrating the degeneracy of the MA spidroin sequence and the common 3-residue motifs.

disordered random coil proteins, reminiscent of intrinsically disordered proteins (IDPs). The very long chain length, sequence redundancy and poor chemical shift dispersion due to the primarily unstructured nature of the proteins make unique resonance assignments for each of the thousands of amino acid residues extremely challenging; nevertheless, by using 3D solution NMR experiments we can still several small repetitive motifs. In order to partially assign the chemical shifts of all 12 resonances, we followed the standard assignment strategy of using HNCACB and CBCAcoNH triple-resonance experiments (Figure 14). This strategy initially permits two-residue assignments for each resonance, which agree very well with the correlated assignment in the intact glands from previous work indicating primarily random coil proteins (data not shown).

In the HNCACB experiment shown in Figure 14 (left), green resonances correspond to the negatively phased $^{13}C\beta$ resonances while red resonances represent positively phased $^{13}C\alpha$. Strong resonances correspond to $^{13}C\alpha/\beta$ resonances from those directly bound to the residue (i) and weak resonances correspond to the preceding (i-1) residue $^{13}C\alpha/\beta$. In the CBCAcoNH experiment, the $^{13}C\alpha/\beta$ pairs correlate only to the i-1 residue. The use of both experiments allowed us to expand our assignments to three residues. Triple-residue assignments were made by correlating pairs of strips from both 3D experiments to each other (Figure 14). Each pair of strips from the CBCAcoNH and HNCACB experiments correlates to an identical ^{15}N slice from the $^{1}H/^{15}N$ HSQC. This provides the initial i-1 to i two-residue assignment. For some of the peaks, considerable spectral overlap exists making it challenging to confidently make more than these two-residue assignments. However, in a few cases, unique $^{13}C\alpha/\beta$ pairs of resonances for a single ^{15}N chemical shift can be found in both spectra, allowing for three residue assignments by comparing both 3D data sets. This provided the three-residue assignments reported in Figure 13.

The chemical shifts of all identified residues correspond very closely to those of random coils, but in a few cases, we observed significant perturbations between the intact gland and the spectra of the silk dope solubilized in 4M urea as a function of protein

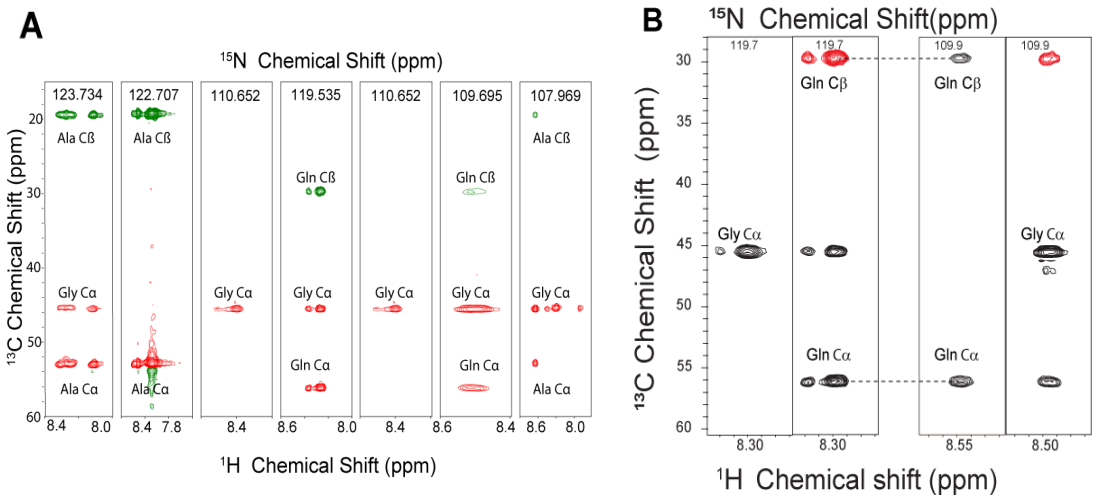

Figure 14. Strip plots from HNCACB experiments showing 2-residue correlations (A). Two residue assignments can be made from this single experiment, but the majority of repeating motifs in the silk sequences are three-residues in length. For this reason we applied a second 3D experiment, CBCACONH, which ties together two amide resonances to a common set of carbon resonances. For some cases, a unique pair could not be assigned due to large amounts of overlap. But in a several cases (example of GQG shown) unique carbon signals could be matched. It is important to note that these are not unique residues, but rather a collection of repeating motifs that have the same triple-residue pattern. In two cases, the published sequence was used to assign sequences which could not

concentration (discussed below). Because the most common motifs in the repetitive core of the spidroins are three residues long, this permits characterization of the backbone structure and dynamics more deeply than previous studies. For example, the GQG motif is very common in the sequence of MaSp1 and MaSp2 although it generally localizes to MaSp1**.** The complete primary protein amino acid sequence of both spidroins is shown in the Appendix, Figure A1, where all the short three residue repeats that are resolved in solution NMR are underlined and highlighted.

In order to get information about the motif-specific dynamics, we measured the MA silk spidroin backbone relaxation parameters, T_1, T_2, and heteronuclear NOEs for the backbone amide nitrogen nuclei. These values report on global tumbling of proteins and local backbone dynamics and serve as an indicator of the level of order along the protein chain. Not all twelve resonances in the original $^1H/^{15}N$ HSQC were sufficiently resolved in the relaxation measurements to be adequately fit to a decay curve. Comparing published values of T_1 and T_2 for intact glands there is a clear and significant increase in the dynamics of the proteins suggesting they exhibit an extended disordered random coil state in 4M urea. That is more dynamic than the native state. This data clearly shows that the bulk relaxation profiles of spidroins in 4M urea are very different from their native state within intact glands but, as expected, show an increase in dynamics at lower protein concentration in the presence of the urea denaturant.

In order to investigate the role of concentration at the same field strength, we performed the T_1 and T_2 experiments in two concentration regimes at 600 MHz, one at 1 wt% and one between 5-7 wt%. The T_1 and T_2 parameters were extracted from a decaying exponential fitting function which can contain one or multiple components. The T_2 times in both concentration regimes fit to a single decaying exponential (as measured by Monte Carlo simulations to estimate error to the 95% confidence level). On the other

hand, T_1 times are more confidently fit to a two-component decaying curve for both concentrations. A fast and a slow component for the T_1 relaxation times is thus, reported in Figure 16. Heteronuclear NOE values are another valuable indicator of protein dynamics. Values for all resolvable resonances are negative, including the AAA peak, which is slightly below zero and thus, more rigid compared to the rest of the spidroin motifs (data not shown). Nonetheless, long relaxation and negative NOE values demonstrate that the spidroins are highly flexible at dilute protein concentration analogous to the MA proteins at native concentration albeit with even faster dynamics.

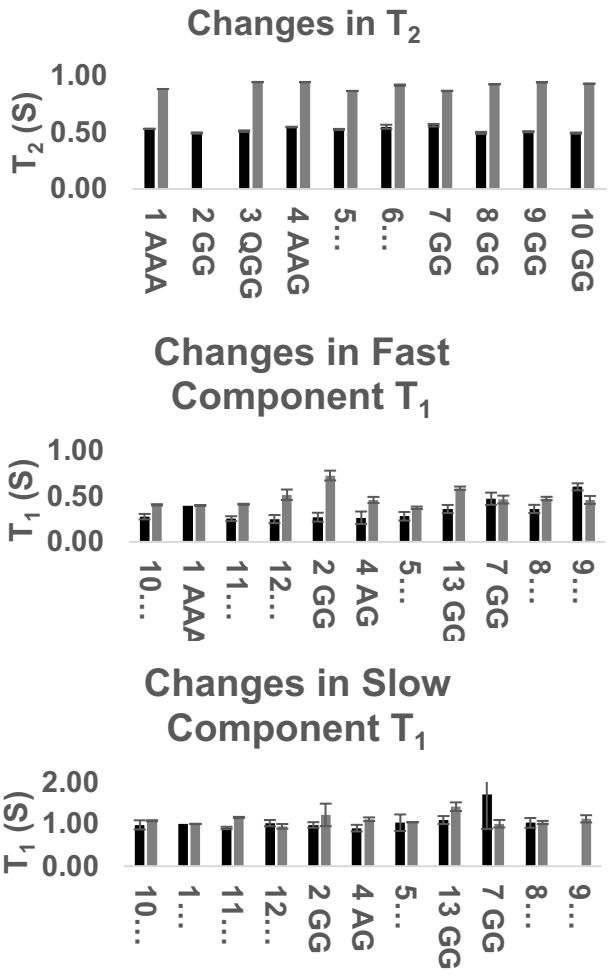

Figure 16. Longitudinal relaxation, T_1, (A), transverse relaxation, T_2, (B) heteronuclear NOEs (C). T_2 values are significantly longer than previously published average values for relaxation on intact glands. Low (~1 wt%) and high (~5-7 wt%) concentration regimes are represented by black and gray bars, respectively.

In order to properly attribute changes in structure and dynamics to either the dissolved MaSp protein monomers or the pre-assemblies, we first needed to determine the protein concentration at which these pre-assemblies dissolve. Due to the high concentration of protein leading to incoherent data, we were unable to use DLS. Instead, we utilized the same approach employed in our previous work, using diffusion NMR to monitor the disappearance of restricted diffusion of our MaSp protein in 4 M urea. Previously, we have used diffusion NMR to determine that the MaSp proteins are restricted in the gland to a volume space of ~ 250 nm after observing a diffusion dependence on Δ and subsequently taking the MSD to calculate the size (reference 1). Additionally, we calculated the size of a single MaSp monomer using dilutions between 0.1-1 wt%, where there is no dependence on Δ and thus free diffusion, and extrapolated to infinite dilution. Modifying this approach slightly, here we measure the diffusion of MaSp proteins at concentrations between native (25-50 wt%) and dilute (1 wt%) conditions, calculating the mean-squared displacement (MSD) and inspecting the MSDs for an abrupt change in slope corresponding to faster (unrestricted) diffusion. At native concentrations, MaSp proteins are restricted in the gland and the MSD is plateaued at

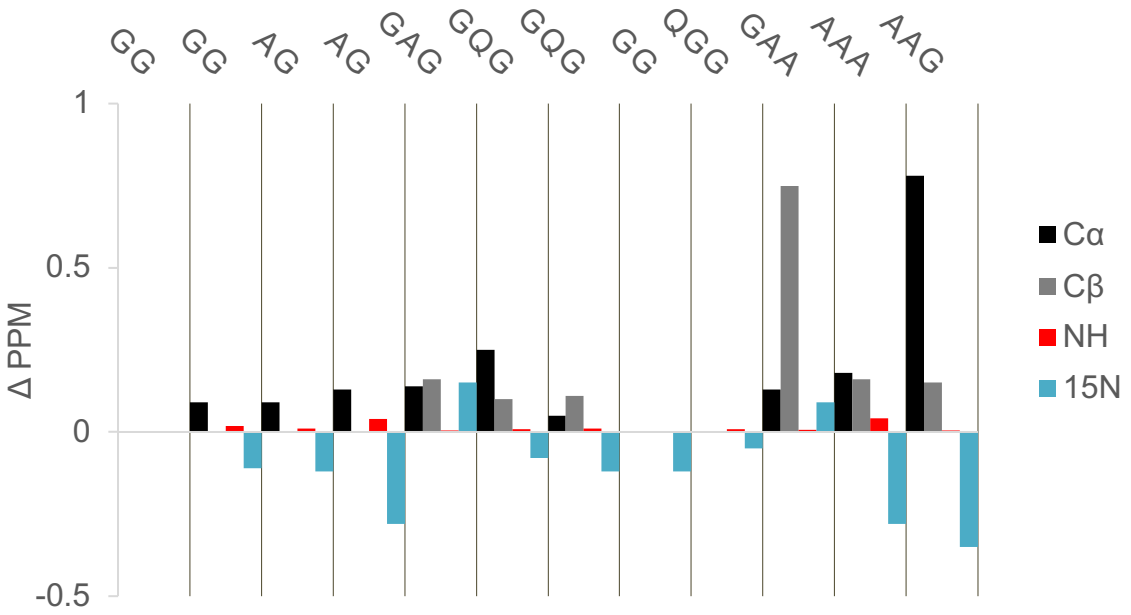

Figure 17. Changes in the chemical shift between the native intact glands and the diluted (~1 wt%) samples are summarized in this chart. The chart is arranged roughly in the order of direction the sequence proceeds so that the glycine-rich regions come before the poly(Ala) regions.

~300 nm. This agrees well with our previously published data showing that in the native gland environment the MaSp proteins are found in pre-assemblies.

By applying typical ^{1}H-detected 2D and 3D protein solution NMR strategies to silk protein solutions, assignments were made for up to three consecutive residues for all of the regions observed in the ^{1}H/^{15}N HSQC spectrum. In fact, the three-residue assignments constitutes 82% of the full sequence of MaSp1 and 50% of the sequence of MaSp2 (Appendix, Figure 1A). This is a tremendous step towards the complete NMR structural and dynamic characterization of the primary spider silk protein and opens the door to continuing investigation under various biochemical conditions (pH, salts, and denaturants). While most of the chemical shifts are nearly identical to those of intact glands, we have identified regions of the proteins that do show significant (~1 ppm) changes in the urea denaturant (Figure 17, 18). These regions flank the poly(Ala) runs of the repetitive spidroin's core. Spider silk fiber is a semi-crystalline polymer with small β-sheet poly(Ala) and poly(Gly-Ala) domains with some Ser that are interspersed throughout an otherwise mostly disordered, loose helical matrix. We rationalize the large chemical shift changes at the edges of these poly(Ala) regions when the spidroins are dissolved in denaturant as disrupting and collapsing of these domains into their native secondary structure which is in agreement with the decreasing sizes that we see as a function of dilution and time in urea with DLS (Figure 12, table 1). Due to the hydrophobic nature of the poly(Ala) motif, we expect it to be preferentially buried and away from the protein surface. Denaturation might cause the poly(Ala) flanking regions (AAG and GAA) to be more exposed to solvent and therefore be unable to form native contacts, which also helps to explain the solubility of these large aggregation-prone proteins.

Dynamic experiments show that dilute solutions in 4M urea have increased T_1, and T_2 times, corresponding to highly flexible unfolded random coils with increased chain dynamics. The increased dynamics can be readily by explained by both the presence of a denaturant and different concentration of the sample, which agrees with diffusion data we previously published on this system (reference 1). Heteronuclear NOE values also indicate increased dynamics in solution. Based on previous results showing primarily monomer-sized populations in dilute solutions (~1% wt) and we believe that our experiments mainly probe this population. However, our data clearly shows that T_1 relaxation parameters are better fit to two-component exponential decays. We interpret this to mean that the larger micelle-like hierarchal assemblies remain stable at a spectroscopically relevant concentration, but decrease in size. The increase in dynamics at higher (but not native) concentrations of 5-7 wt% may be due to increased dynamics in a non-equilibrium population. Further, the analysis of concentration dependence in order to truly understand this relationship is the subject of future studies.

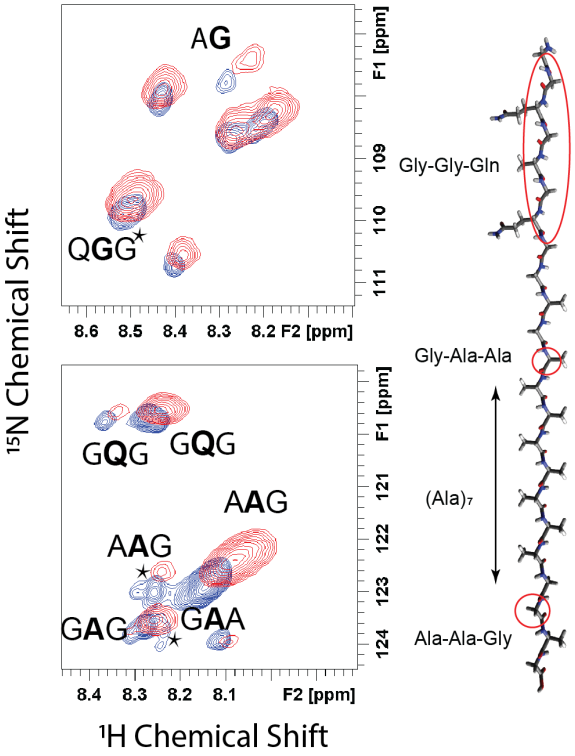

Figure 18. The $^{1}H/^{15}N$ HSQC NMR spectra of $^{13}C/^{15}N$-Ala-labeled Ma spider silk protein within intact glands excised from *L. hesperus* spiders. The Gly and Ala region of the spectrum are expanded in the top and bottom spectra, respectively. The silk dope within intact glands at native concentration (~35 wt%) is shown in red and dope dissolved in 4M urea (~5 wt% protein) in blue. MaSp1 backbone chain is shown to the right. Large chemical shift perturbations are observed for Gly-Ala-Ala and Ala-Ala-Gy domains and the Gly-Gly-Gln and $(Ala)_n$ regions only display negligible or minor changes.

Understanding the nature of spider silk proteins in solution, prior to fiber formation, is crucial to elucidating the spinning process, which in turn is a requirement for successfully producing synthetic spider silk fibers with native properties. Solution NMR is a powerful tool for probing atomic and molecular level interactions both in terms of structure and dynamics. Recent work by our group has shown that spidroins assume a hierarchical superstructure within the MA glands that is surprisingly absent of virtually all secondary structure in the repetitive core. Here we have laid the groundwork for beginning to understand the intermolecular interactions responsible for facilitating these large silk protein assemblies. By diluting the silk protein in 4M urea, we are able to solubilize the native silk dope with all associated components, maintain its stability for at least 48 hours and monitor the disassembly of these protein superstructures. These investigation are continuing in earnest with our new grant (awarded June 2020).

5. Personnel Supported:

1) Gregory P. Holland (PI, SDSU), Supported one month of summer salary per year.

2) Jeffery L. Yarger (co-PI, ASU), Supported two weeks of summer salary per year.

3) David Onofrei (Ph.D. Student, Research Assistant, SDSU), Supported 2 years.

4) Brandon Blass (M.S. Student, Research Assistant, ASU), Supported 2 year.

5) Aleksandar Lazaric (Ph.D. Student, Research Assistant, ASU), Supported 1 year.
6) Dillan Stengel (Ph.D. Student, Research Assistant, SDSU), Supported 1 year.

6. Publications:

1) Parent, L.R., Onofrei, D., Xu, D., Roehling, J.D., Addison, J.B., Froman, C., Amin, S.A., Cherry, B.R., Yarger, J.L., Gianneschi, N.C., Holland, G.P. "Hierarchical Spidroin Micellar Nanoparticles as the Fundamental Precursors of Spider Silks" *Proc. Natl. Acad. Sci. USA* **2018**, *115*, 11507-11512.
2) Addison, B., Onofrei, D., Stengal, D., Blass, B., Brenneman, B., Ayon, J., Holland, G.P. "Spider Prey-wrapping Silk is an □-helical coiled-coil/□-sheet Hybrid Nanofiber" *Chem. Commun.* **2018**, *54*, 10746-10749.
3) McGill, M., Holland, G.P., Kaplan, D.L. "Experimental Methods for Characterizing the Secondary Structure and Thermal Properties of Silk Proteins", *Macromol. Rapid Commun.* **2018**, 1800390.
4) Yarger, J.L., Cherry, B.R., Van Der Vaart, A. "Uncovering the Structure-Function Relationship in Spider Silk" *Nature Review Materials* **2018**, *3*, 18008.
5) Guo, C., Zhang, J., Jordan, J.S., Wang, X., Henning, R.W., Yarger, J.L. "Structural Comparison of Various Silkworm Silks: An Insight into the Structure-Property Relationship" *Biomacromolecules* **2018**, *19*, 906-917.
6) Parent, L.R., Onofrei, D., Xu, D., Roehling, J.D., Addison, J.B., Froman, C., Amin, S.A., Cherry, B.R., Yarger, J.L., Gianneschi, N.C., Holland, G.P. "Hierarchical Spidroin Micellar Nanoparticles as the Precursors of Spider Silks", *Microscopy and Microanalysis* **2019,** *25*, 1346-1347.
7) Guo, C. and Yarger, J.L. "*NMR Characterization of Silk*" p. 420-456 in *NMR* Methods for Characterization of Synthetic and Natural Polymers **2019**, Royal Society of Chemistry.
8) Addison, D., Stengal, D., Bharadwaj, V.S., Happs, R.M., Doeppke, C., Wang, T. Bomble, Y.J., Holland, G.P., Harman-Ware, A.E. "Selective One-dimensional ^{13}C-^{13}C Spin Diffusion Solid-state Nuclear Magnetic Resonance Methods to Probe Spatial Arrangements in Biopolymers Including Plant Cell Walls, Peptides and Spider Silk", *J. Phys. Chem. B* **2020**, *124* 9870-9883. ***[Made the Cover]***

9) Stengal, D., Addison, J.B., Onofrei, D., Huynh, N.U., Youssef, G., Holland, G.P. "Hydration-induced β-sheet Crosslinking of α-helical-rich Spider Prey-wrapping Silk**"** *Adv. Funct. Mater.* **2020,** *Accepted.*

7. Interactions/Transitions:

a. Participation/presentations at Meetings, Conferences, Seminars:

1) Holland, G.P. and Onofrei, D., "X-detect solution NMR for Investigating the Structure and Dynamics of Spider Silk Pre-assemblies" American Chemical Society 260th National Meeting, San Francisco, CA (2020). ***[Invited]*** *Held Virtually Due to the Pandemic*
2) Holland, G.P., "The Molecular Mechanisms of Spider Silk Assembly" DOD-AFOSR (Natural Materials and Systems) Program Review, Fort Walton Beach, FL (2019).
3) Holland, G.P. "The Hierarchical Assembly of Spider Silk: Connecting the Molecular and Nanometer Length Scales" Frontiers in Soft Matter and Macromolecular Networks, San Diego, CA (2019). ***[Invited]***
4) Holland, G.P. Onofrei, D., Stengel, D., Addison, J.B "Water-induced □-sheet Crosslinking of α-helix Rich Spider Prey Wrapping Silk" American Chemical Society 257th National Meeting, San Diego, CA (2019).
5) Onofrei, D., Stengel, D., Addison, J.B., Holland, G.P. "NMR Characterization of Spider Silk Protein Nanoparticle Pre-assemblies" American Chemical Society 257th National Meeting, San Diego, CA (2019).
6) Davidowski, S.K., Addison, J.B., Holland, G.P., Yarger, J.L., "Elucidation of the Molecular Structure and Dynamics of Egg Sac Spider Silks Using Solid-state NMR" American Chemical Society 257th National Meeting, San Diego, CA (2019).
7) Holland, G.P. "The Molecular Mechanisms of Spider Silk Assembly", Department of Exobiology, NASA Ames Research Center, Mountain View, CA (2019). ***[Invited]***
8) Holland G.P. and Addison B. "Combining NMR, Electron Microscopy and Computational Techniques to Elucidate the Molecular Structure and Assembly of Spider Silk", Computational Sciences Colloquium, San Diego State University, San Diego CA (2019). ***[Invited]***
9) Holland, G.P. "The Molecular Mechanisms of Spider Silk Assembly", Departmental Seminar – Chemical and Biomolecular Engineering and Materials Science and Engineering, University of California Irvine, Irvine, CA (2019). ***[Invited]***
10) Holland, G.P., "The Molecular Mechanisms of Spider Silk Assembly" DOD-AFOSR, 2312 EX and DX (Natural Materials, Systems and Extremophiles) Program Review, Fort Walton Beach, FL (2018).

11) Holland, G.P. and Addison, B. “Combining NMR and Computational Techniques to Elucidate the Molecular Structure and Assembly of Spider Silk”, Computational Sciences Colloquium, San Diego State University, San Diego, CA (2018).

12) Holland, G.P. “Micellar Protein Nano-Assemblies in the Native Silk Dope of Black Widow Spiders”, 4th Functional Polymeric Materials Conference, Nassau, Bahamas (2018).

13) Onofrei, D., Stengel, D., Valdez, G., Villalba, A. Addison, B., Holland, G.P. “Using NMR to Probe the Structure Dynamics and Assembly of Spider Silk Fibers”, 255th American Chemical Society National Meeting, New Orleans, Louisiana (2018).

14) Yarger, J.L. “The Physics of Spider Silk and Related Biopolymers” Physics Colloquium, Washington State University, Pullman, WA, Canada (2018).

15) Yarger, J.L. “Silk: Nature’s Diverse Copolymer” Physics Colloquium, Colorado State University, Fort Collins, CO, USA (2018).

16) Holland, G.P. “Using NMR to Probe the Structure, Dynamics and Assembly of Spider Silk Fibers”, American Chemical Society 255th National Meeting, New Orleans, LA, USA (2018).

17) Yarger, J.L. “Frontiers in Amorphous Physical Chemistry” Frontiers in Physical Chemistry Award and University Talk, University of Wyoming, Laramie, WY, USA (2018).

18) Yarger, J.L. “Amorphous Biomaterials” BioPhest, University of Arizona, Tucson, AZ, USA (2018).

19) Onofrei, D., Larson, T., Villalba, A., Holland, G.P. “Probing Silk Protein Oligomeric Assemblies in Spider Silk Glands with NMR Diffusion Measurements and Cryo-EM” The 29th Annual CSU Biotechnology Symposium, Santa Clara, CA (2017).

20) Holland, G.P. “The Molecular Mechanisms of Spider Silk Assembly”, Sheffield Silk Conference, Halifax Hall, University of Sheffield, Sheffield, England (2017).

21) Holland, G.P. “The Molecular Mechanisms of Spider Silk Assembly” Departmental Seminar – Chemistry and Biochemistry, Long Beach State University, Long Beach, CA, USA (2017).

22) Yarger, J.L. “Spider Silk Proteins and Polymers” Biochemistry Seminar, University of Texas Austin, Austin, TX, USA (2017).

23) Yarger, J.L. “Structure-Function of Silks – Nature’s Versatile Polymer” Physics Colloquium, University of British Colombia, BC, Canada (2017).

24) Yarger, J.L. “Laser-Sealing of Soft Tissue Using Plasmonic Silk Nanocomposites” Biomedical Engineering Society, Phoenix, AZ, USA (2017).

b. Consultive and Advisory Functions: None
c. Technology Assists, Transitions, and Transfers: None

8. New discoveries, inventions, or patent disclosures: None

9. Honors/Awards:

1) Holland, G.P. SDSU, The 2018 CoS Outstanding Faculty Award for Teaching (2018)
2) Holland, G.P. SDSU, The 2019 CoS Outstanding Faculty Award for Research (2019)

!0. Appendix (Figure A1)

MaSp1

MTWSTRLALSFLFVLCTQSLYALAQANTPWSSKANADAFINSFISAASNTGSFSQDQMEDMSLIGNTLMAAMDNMGGRITPSKLQALDMAFASSVAEIAASEGGD
LGVTTNAIADALTSAFYQTTGWNSRFISEIRSLIGMFAQASANDVYASAGSSGGGGYGASSASAASASAAAPSGVAYQAPAQAQISFTLRGQQPVSYGOGGAGPG
GAGAAAAAAAAGGAGGGOGGGYGOGGYGOGGAGOGGSGAAAAAAAAGGTGOGGAGOGGAGAAAAAAAGGAGOGGOGGYGOGGYGOGGTGOGGAG
AAAAAAAGGAGOGGOGGYGOGGYGOGGYGOGGSGAAAAAAAAGGAGOGGOGGYGOGGYGOGGAGOGGAGAAAAAGGAGOGGYGRGGAGOGGAA
AAAAAAAGAGOGGYGGQGAGOGGSGAAAAAAAAGGAGOGGOGGYGOGGYGOGGSGAAAAAAAAGGAGOGGOGGYGOGGYGOGGAGOGGAGAAAAAA
AAGGAGOGGOGGYGOGGYGOGGAGOGGAGAAAAAAAGGAGOGGOGGYGOGGYGOGGAGOGGAGAAAAAAAAGAGOGGOGGYGOGGAGOGG
AAAAAAAAAGGAGOGGYGRGGAGOGGAAAAAGAGOGGYGGQGAGOGGAGAAAAAAAAGGAGOGGOGGYGRGGYGOGGAGOGGAGAAAAAAAAGGAG
OGGOGGYGOGGYGOGGAGOGGAAAAAAAAGGAGOGGYGRGGAGOGGAAAAAAAAAGAGOGGYGGQGAGOGGAGAAAAAAAAGGAGOGGOGGYG
GOGGAGOGGAAAAAAAGGAGOGGYGRGGAGOGGAAAAAGAGOGGYGGQGAGOGGAGAAAAAAAAGGAGOGGOGGYGRGGYGOGGAGOGGAGAAAA
AAAAGAGOGGOGGYGOGGYGOGGAGOGGAAAAAAAAAGGAGOGGYGRGGAGOGGAAAAAAAAAGSGOGGYGGQGAGOGGAGAAAAAAAAGGAGOGGOGG
OGGYGRGGYGOGGAGOGGAGAAAAAAAGGAGOGGOGGYGOGGYGOGGAGOGGAAAAAAAAGAGOGGYGGQGAGOGGAGAAAAAAAAGGAGOGGOGGYG
GOGGAGOGGAGAAAAAAAAGAGOGGOGGYGOGGYGOGGAGOGGAAAAAAAAGGAGOGGYGRGGAGOGGAAAAAGAGOGGYGGQGAGOGGAGAAAA
AAAAGGAGRGGOGGYGRGGYGOGGAGOGGAGAAAAAAAAGGAGOGGOGGYGOGGYGOGGAGOGGAAAAAAAAGGAGOGGYGRGGAGOGGAAAAAG
AGOGGYGGQGAGOGGAGAAAAAAAAGGAGOGGYGRGGYGOGGAGOGGAGAAAAAAAAGAGOGGOGGYGOGGYGOGGAGOGGAGAAAAAAAAGGAG
GOGGYGRGGAGOGGAAAAAAAAAGSGOGGYGGQGAGOGGAGAAAAAAAAGGAGOGGOGGYGGGGYGOGGAGOGGAGAAAAAAAAGAGOGGOGGYGQ
GGYGOGGAGOGGAAAAAAAAAGGAGOGGYGRGGAGOGGAAAATGAGOGGYGGQGAGOGGAGAAAAAAAAGGAGOGGOGGYGRGGYGOGGAGOGGAG
AAAAAAAGGAGOGGOGGYGOGGYGOGGAGOGGAAAAAAAAGGAGOGGYGRGGAGOGGAAAAAAAAAGGAGOGGYGGQGAGOGGAGAAAAAAAAGGAG
OGGOGGYGRGGYGOGGAGOGGAGAAAAGAGOGGOGGYGOGGYGOGGAGOGGAAAAAAAAAAGGAGOGGYGGYGOGGAGAAAAAASGPGQIYYGPQS
VAAPAAAAASALAAPATSARISSHASALLSNGPTNPASISNVISNAVSQISSSNPGASACDVLVQALLELVTALLTIIGSSNIGSVNYDSSGQYAQVVTQSVQNAFA

MaSp2

MTTMNWSTRLVLSILVVLCTQSLCALGQANTPWSSKENADAFIGAFMNAASQSGAFSSDQIDDMSVISNTLMAAMDNMGGRITQSKLQALDMAFASSVAEIAVA
DGQNVGAATNAISDALRSAFYQTTGVVNNQFITGISSLIGMFAQVSGNEVSYSSAGSSSAAASEAVSAGQGPAAQPVYAPSGASAAAAAASGAAPAIQQAYERGG
SGSAAAAAGSGPSGYGQGAGGPGGAGAAAGAAAAGGSGPGGYGQGPAAYGPSGPSGQQGYGPGGSGAAAAAAAAAGSGPSGYGPGAGGPGGAGAAAAAA
AAGGSGPGGYGQGQASYGPSGPSGQQGYGPGGSGAAAAAAAAGSGPSGYGPGAAAAAAGSGPRGYGPRGPGGAGAA
ATAARGSGPGGYGQGPAGYGTSGPSRQQGYGPGGSGAAAAAAAAAGGAGPGRQQGYGPGGSGAAAATAAGGPGYVGQQRYGPGGAGAAAAAAAGSAGPS
RQQAYGPGGSGPAAATAAAGSGPSGYGPGASGPVGADAAAAAATGSAGPGRQQAYGPGESGAAAAAASGAGPGRQLGYGPGGSGAAAAAAAGGPGYGGQQ
GYGPGGAGAAAAAAAGGAGPGRQQTYGPGGSGAAATAAGGSGPGGYGQGPSGPGGQQGYGPGGSGAAAAAAAGEAGPGRQQGYGPRGSGAAAAA
AAGGPGYGGQSGYGPGGAGAAAAAAAGGAGPGRQQEYGPGGSGAAAAAAAAAGSGPSGYGPGAAGPIGPGGAGAAAAGGSGPVGYGQGPSGYGASGTGGE
QDYGPGGSGAAAAAAAAAGGAGPGRQQGYGPGGSGAAAAAAAGGPGYGGQQGYGPGGAGAAAAAAAGGAGPGRQQPYGPGGAGAAAAAAGGSGPGGYG
QGPSGYGASGPGGQQGFGPGGSGAAAAAAAGGAGPGRQQGYGPGGSGAAAAAGGTGYGGQQGYGPGGAGAAAAAAAAGAGPGRQQEYGPGGTGAAAAAA
AAAGSGPSGYGQGAAGPSGPGGEGTAAAAAAAGGSGPGGYGQGPSGYSASGPGGQQGYGPGGSGLAAAAAAAAGGAGTGRQQGYGPGGSGAAAAAAAVGP
GYGGQQGYGPGGAGAAAAAAAGGAGPGRQQAYGPGGSGATAAAAVAGSGPSGYGPGGAGAAAAAAAGGAGPGRQQAYGPGGSGAAAAAASGAGPGRQQ
VYGPGGSGAAAAAAAGGPGYGGQQGYGPGGAGAAAAAAAGGAGQGTRQAYGPGGSGAAAAAAGGPGPSGYGPGAAGPGGAGAAAAGSGPSGYEPGAAGPGGAGAAAA
AAAVGAGPGRQQAYGQGGSGAVAAAAAGGPGYGGQQGYEQGGAGAASAAAAGGEGPARQQAYGPGGSGAAAAAAGGAGPGRQQGYGPGSSGAAAAAAAA
GGPGYGGQQGYGPGGAGAAAAAAAGGAGPGRQQAYGPGGSGAAAAAAAGTGPSGYGPGAAGPGGAGAAAAAAAGSAGPGRQQAYGPGGSGAAAAAAAG
GPGYGGQQGYGPGGAGAAAAAAAGGAGPGTQQAYGPGGSGAAAAAAAAAGGAGPDRQQGYGPGSSGAAAAAAAGGPGYGGQQGYGPGGAGAAAAAAAA
AGPGPSGYGPGGAGAAAAAAAAGGSGPGGYGQGPSGYSASGPGGQQGYGPGGSGLAAAAAAAAGGAGTGRQQGYGPGGSGAAAAAAAGGAGPGRQQGYGP
PGGAGAAAAAAAGGAGPGRQQAYGPGGSGATAAAAAAGSGPSGYGPGGAGAAAAAAAGGAGPGRQQAYGPGGSGAAAAAASGAGPGRQQVYGPVGSGAA
AAAAAGGPGYGGQQGYGPGGAGAAAAAAAGGAGQGTRQAYGPGGSGAAAAAAGPGPSGYGPGAAGPSGPGLAGAAAAAAAGGSGPGGNGQRPSGYGQSG
PGGQQGYGPGGSGAAAAAAAAGGAGPGRQQGYGPGSSGAAAAAAAGGPGYGGQQGYGPGGAGAAAAAAAGGAGAGRQQAYGPGGSGAAAAGSGPSGYESGAAGPGGAGAAAAAAAVGAGPGR
QQAYGQGGSGAVAAAAAGGPGYGGQQGYEQGGAGAASAAAAGGEGPARQQAYGPGGSGAAAAAAGGAGPGRQQGYGPGSSGAAAAAAAGGPGYGGQQG
YGPGGAGAAAAAAAGGAGPGRQQAYGPGGSGAAAAAAAGTGPSGYGPGAAGPGGAGAAAAAAAGSAGPGRQQAYGPGGSGAAAAAAAGGPGYGGQQGY
GPGGAGAAAAAAAGGAGPGTQQAYGPGGSGAAAAAAAAAGGAGPDRQQGYGPGSSGAAAAAAAGGPGYGGQQGYGPGGAGAAAAAAAAAGPGPSGYGP
GGAGAAAAAAAAGGSGPGGYGQGPSGYGPSGPGGQQGNGPGGSGAAAAAAAGGAGPGRQQGYGPGGAGAAAAAAGGPGYGGQQGYGPGGAGAAAAAAAAAG
AGGAGPGRQQAYGPGGAGAAAAAAAAGPGPSGYGPGASGPSGTGGAGAAAAAAAAGGSGPGGYGQGASGYGPSGPGGQQGYGPGGSGAAAAAAAAGG
AGPGRQQGYGPGSSGAAAAAAAGGPGYGGPQGYGPGGAGAAAAAAAGGAGPGRQQAYGPGGSGAAAAAAGSGPSGYGPGAAGPGGTGAAAVAAAGGAGP
GRQQAYGPGGSGAAAAAAAGGPGYGGQQGYGPGGAGAAAAAAAGGAGPGTQQLYGPGGSGAAAAAAAGSGPSGYGPGAAGPSGPGGAGAAAAAASAG
GSGPGGYGQGPSGYGPTGPVGQQGYGPGGSGAAAAAAAAGGAGPGRQQGYGPGSSGAAAAAAGGPGYGGQQGYGPGGAGAAAAVAAGGAGPGRQQGY
GPGSSGAAAAAAAGGPGYGGQQGYGPGGAGAAAAVAAGGAGPGRQQGYGPGSSGAAAAAAAGGPGYGGQQGYGLGVAGAAAAVAAGGAGPGRQQAYGP
GGSGAAAAAAAGSGRSGYGPGAAGTGGAGAAAAAAAGGAGSGRQQAYGPGGSGAAAASAAGGPGYGGQQGYGPGGAGAAAAAAGGAGPGTQQAYGPG
GSGAAAAAAAASGPGPSGYEPGAAGPSGPAGAGAAAAAAAAAGGSGPGGYGQGPSGYGPSGPGGQQGYGPGGSGAAAAAAAAGGAGPGRQQGYGQGSSGA
AAAAAAGGPGYGGQQVYGPGGAGAAAAVAAGGAGPGRQQAYGPGGSGAAAGSGPSGYGPGAAAAAAAGGAGPGRQQAYGPGGSGAAAAAAAGGPGYGG
QQGYGPGGAGAAAAAAAGGSGPGGYGQGPSGYGPSGSGGQGYGQGGSGAAAAAAGGAGPGRQQGYGPGSSGAAAAAAGGPGFGQGQPAGYGPSGPGGQQGYGPGASGAAAAAA
AAGGAGPGRQQAYGPGGSGAAAAAAAAAGSGPSGYGPSAAGPSGPGGSGAAGGSGPGGFGQGPAGYGPSGPGGQQGYGPGASGAAAAAA
YVPSSVASSAASAASALSSPTTHARISSHASTLLSSGPTNAAALSNVISNAVSQVSASNPGSSSCDVLVQALLEIITALISILDSSSVGQVNYGSSGQYAQIVGQSMQQ
AMG

Figure A1. The complete sequence of the two major spidroin components of black widow MA silk, MaSp1, and MaSp2. The highlighted regions show all motifs that can be assigned from the 3D NMR experiments. Underlined regions are partial assignment as detailed in the text.